High Current Hollow Cathode Plasma Plume Measurements

IEPC-2013-076

33rd International Electric Propulsion Conference,
The George Washington University, Washington, D.C., USA
October 6–10, 2013

Robert E. Thomas* and Hani Kamhawi†
NASA Glenn Research Center, Cleveland, OH, 44135, USA

George J. Williams, Jr.‡
Ohio Aerospace Institute, Cleveland, OH, 44135, USA

Plasma plume measurements are reported for a hollow cathode assembly (HCA) operated at discharge currents of 50, 70, and 100 A at xenon flow rates between 19 - 46 sccm. The HCA was centrally mounted in the NASA-300MS Hall Thruster and was operated in the "spot" and "plume" modes with additional data taken with an applied magnetic field. Langmuir probes, retarding potential analyzers, and optical emission spectroscopy were employed to measure plasma properties near the orifice of the HCA and to assess the charge state of the near-field plasma. Electron temperatures (2-6 eV) and plasma potentials are consistent with probe-measured values in previous investigations. Operation with an applied-field yields higher discharge voltages, increased Xe III production, and increased signals from the 833.5 nm C I line. While operating in plume mode and with an applied field, ion energy distribution measurements yield ions with energies significantly exceeding the applied discharge voltage. These findings are correlated with high-frequency oscillations associated with each mode.

Nomenclature

B	= magnetic field strength, T	q	= ion charge, C
B_o	= magnetic field at thruster full power, T	r	= radial position from centerline, m
c	= speed of light, m/s	T	= transition intensity
E	= energy, J	T_e	= electron temperature, K
h	= Planck's constant, J-s	V	= voltage, V
I	= current, A	z	= axial distance from keeper face, m
$I(\lambda)$	= wavelength intensity at frequency λ	α	= doubly charged ion fraction
k	= Boltzmann constant, J/K	λ	= wavelength, m
k_e	= electron collision excitation rate, $m^3\ s^{-1}$	ν	= frequency, Hz
k^q_{ion}	= collision excitation rate with ions of charge q, $m^3\ s^{-1}$	σ_e	= electron cross section, m^2
M	= ion mass, kg	σ_{ion}	= ion cross section, m^2
m_e	= electron mass, kg	Subscripts	
n_0	= neutral particle number density, m^{-3}	D	= discharge
n_e	= electron number density, m^{-3}	K	= keeper

*Research Engineer, Propulsion and Propellants Branch, robert.e.thomas@nasa.gov.
†Research Engineer, Propulsion and Propellants Branch, hani.hamhawi-1@nasa.gov.
‡Senior Scientist, Propulsion and Propellants Branch, GeorgeWilliams@oai.org.

I. Introduction

NASA is currently pursuing high-power electric propulsion systems that can reduce launch vehicle size and enable the transportation of large payloads. A number of high-power NASA Glenn Research Center (GRC) Hall thrusters have been designed and tested, which include the NASA-300M, NASA-300MS and the NASA-457Mv2.[1–3] Missions utlizing these thrusters will require high-current (50 - 100 A), long lifetime (> 30 khr) hollow cathodes assemblies (HCAs). This paper describes current work at GRC to develop HCAs capable of meeting these requirements, with an emphasis on characterizing the near-field plasma plume region. Of particular interest are the presence of high-energy ions, which have been correlated to excessive erosion of the cathode keeper plate.[4–8] The extended life test of the NSTAR ion engine, which ran for 30,352 hours, illustrates the magnitude of this problem. While the thruster was still operational at the end of the test, the keeper face plate had completely eroded and the cathode assembly was nearing the end of life.[9]

The current study presents ion energy distributions, emission spectra, and high-frequency oscillation data for a GRC-developed HCA over a range of operating conditions. The performance of three GRC-developed HCAs has recently been documented.[10] Two configurations (designated Config. 1 and 2) utilized a novel emitter design and are shown in Fig. 1. The Config. 2 assembly had a slightly larger orifice plate diameter and shorter emitter length than Config. 1. The third HCA was largely identical to the NEXT ion engine discharge cathode. The Config. 2 HCA operated at lower temperatures (which is correlated to longer emitter lifetime), therefore all data presented in this report utilizes the Config 2 HCA.

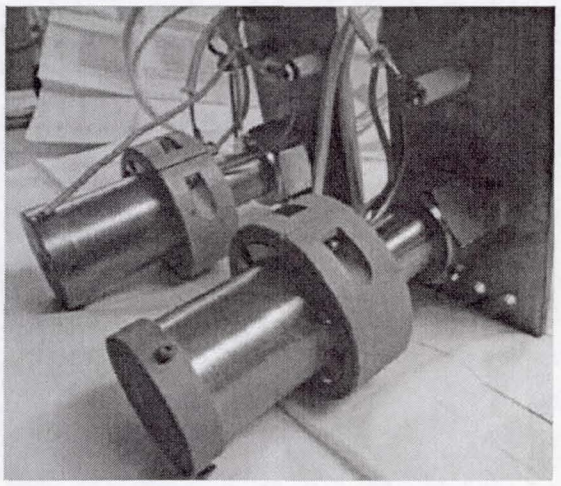

Figure 1: NASA GRC-developed high-current cathode assemblies.

The current investigation utilizes an experimental set-up similar to the one described in Ref. [10], with two notable changes. To decrease sputter erosion, the keeper material has been changed from molybdenum to graphite. Additionally, the HCA is now centrally mounted in the NASA-300MS Hall thruster. The NASA-300MS utilizes a magnetic field configuration designed to significantly limit discharge channel wall erosion, which is the life-limiting mechanism for traditional Hall thrusters. The magnetic shielding concept is described in Ref. [11]. Performance data and a detailed overview of the NASA-300MS is presented in Ref. [3]. Far-field plume measurements and interior probe data of the thruster are presented in Refs. [12] and [13], respectively.

The present study presents preliminary data on the Config. 2 HCA with and without an applied magnetic field. The following section describes the experimental apparatus. Baseline data is then presented with and without an applied magnetic field. The objectives of the work are to:

- assess HCA operation and determine the plasma properties in the near-field plume region in a representative Hall-thruster set-up;
- measure the ion energy distribution and correlate it with specific operating conditions; and

- implement optical emission spectroscopy (OES) interrogation techniques[14–17] to determine xenon plasma properties and relative keeper erosion.

II. Apparatus

A. Facility

Testing was conducted in Vacuum Facility 7 at NASA GRC. The facility is 3 m in diameter with a length of 5.5 m. It is equipped with five 0.9 m diameter oil diffusion pumps with a base pressure of 3.3 $\times 10^{-5}$ Pa (2.5 $\times 10^{-7}$ torr). The pressure during operation was monitored using a hot-cathode ionization gauge mounted near the HCA and the pressure during operation did not exceed 1.9 $\times 10^{-3}$ Pa (1.4 $\times 10^{-5}$ torr, corrected for Xe). A commercial mass flow controller was used to provide high-purity xenon to the HCA. Commerical power supplies were used to control the heaters, keeper, magnetic field, and anode.

B. Hollow Cathode Assembly Configuration

As noted earlier, the electrically floating HCA was centrally mounted in the NASA-300MS Hall thruster. This was done to generate the magnetic field countours the HCA experiences during nominal Hall thruster operation. A 20 cm diameter molybdenum cylindrical anode was placed 20 cm downstream of the HCA; this configuration was consistent with prior testing.[10]

C. Diagnostics

The experimental set up showing the centrally mounted HCA, anode, and plasma diagnostics is shown in Fig. 2. Differential probes were used to measured the discharge voltage and the keeper voltage. A Hall probe was used to measure the discharge current. The signals from the probes were recorded using a 100 Mhz oscilloscope. A description of the electrostatic and optical probes is in the following subsections.

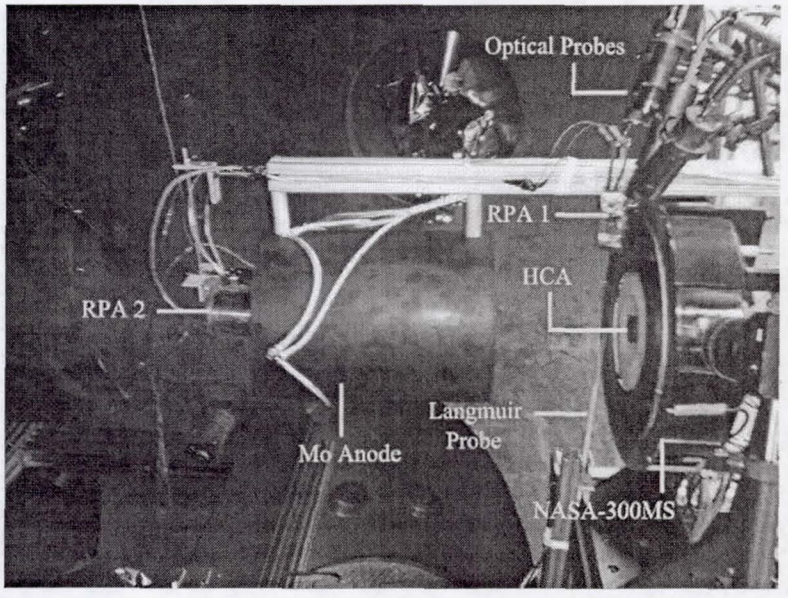

Figure 2: Photograph of HCA experimental set-up.

1. Electrostatic Probes

Two retarding potential analyzers (RPAs) were used to ascertain the ion energy distribution. The RPAs utilize a four-grid design that equally biases the electron suppression and repelling grids with respect to

facility ground while the ion retarding grid is swept. The two probes were located at fixed positions from the HCA. The on-axis RPA was located 40 cm from the keeper face ($z = 40$ cm), while the radially postioned RPA was located 10 cm from the center-line ($r = 10$ cm, $z = 1.5$ cm). A mechanical shutter shielded the probes when data was not being collected. A single Langmuir probe was mounted onto a 2 axis ball-screw driven motion table system, and was physically swept to obtain radial profiles of the electron temperature and plasma potential. The Langmuir probe has a length of 2.5 mm and a diameter of 0.25 mm. The probe circuitry is described in Ref. [18] and the data was analyzed using standard probe theory.[19] Raw traces from the RPA and Langmuir probe are shown in Fig. 3.

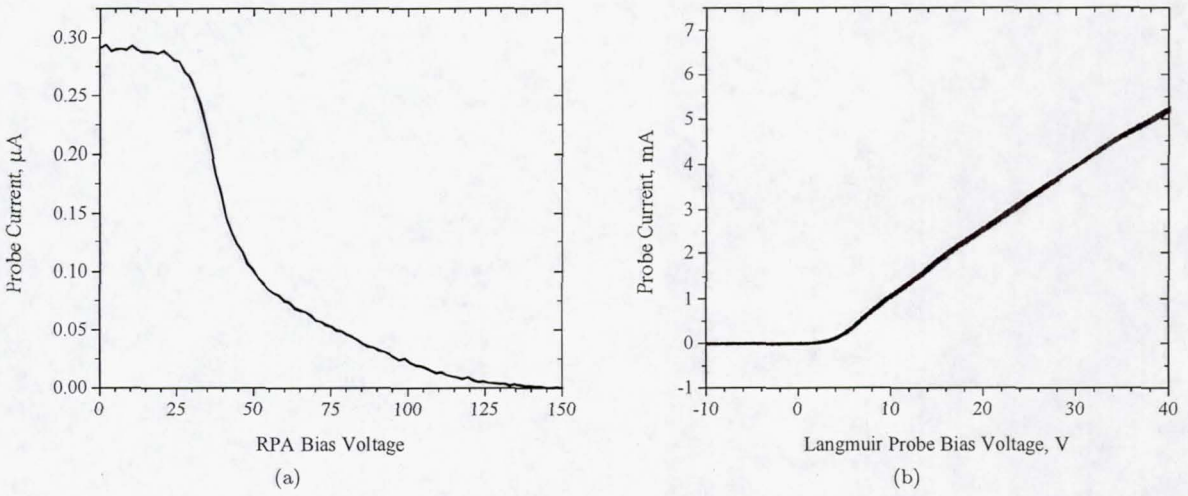

Figure 3: Raw signals of the (a) radially-positioned RPA probe and (b) Langmuir probe ($r = 10$ cm) at a discharge current of 100 A and flow rate of 46 sccm.

2. Optical Probe Description

Optical probes were used to ascertain xenon plasma properties and to investigate graphite keeper erosion. The probes were constructed using 2.5 cm diameter ultraviolet (UV)-silica lenses and flat protective silica windows, optical tubes, and fiber optic connections. Lenses matched the acceptance angle of the 400 μm diameter fiber optic cables and allowed adjustment of the focal point. Single-fiber, metal jacketed fiber optic cables coupled the probes through vacuum feedthroughs to digital spectrometers and photodiodes located external to the vacuum chamber. As seen in Fig. 2, the probes were mounted outside of the radius of the cylindrical anode, roughly 40 cm radially from the centerline of the HCA.

One of the limitations of OES is that light is collected from the entirety of the collection volume downstream of the probe. The probes were focused into collection volumes a few millimeters thick. Because the probes will integrate the signal through the plasma, a tighter focus was not warranted. Three probes interrogated the plasma at the orifice of the keeper, integrating the signal over the bulk of the plasma volume. One of these was connected to a high-speed photodiode which enabled correlation of optical oscillations to current and voltage oscillations. The other two fed UV and infrared (IR) digital spectrometers enabling simultaneous measurement of both spectral ranges. Ultraviolet data were used to correlate xenon charge states. Infrared data were used to calculate electron temperatures using the emission cross sections supplied by Chiu.[20]

The probes were calibrated before and during testing. A standard Xe lamp was placed at the same distance as the location of measurement in the cathode for each probe and spectral data were recorded using the entirety of the probe-fiber system. This measured the transmission function of the different probe assemblies which was used in the reduction of the data. Calibrations were performed during a test sequence by recording spectra at repeated thruster operating conditions. No significant changes in line intensities were noted.

3. Optical Probe Theory and Modeling

A simple collisional radiative model has been exercised to correlate the xenon spectra to plasma properties. It assumes all excitation occurs through collisions and all emission is governed by natural relaxation. Because there are several metastable states within the xenon spectra, a corona model cannot be applied reasonably without relatively high electron temperatures (i.e. $T_e > 40$ eV). Additionally, collisional-radiative models require knowledge of the rate coefficients associated with these transitions over a large number of possible transitions. In general for xenon these are not known. Recent studies have experimentally determined the rate coefficients associated with Xe I and Xe II for a few transitions in the near infrared and in the visible spectrum. In particular, Chiu[20] has developed effective excitation cross-sections that experimentally convolve the possible transitions enabling a relatively simple set of equations for the collision excitation rates

$$k_e = \int_0^\infty 2E\sqrt{\frac{2}{\pi(kT_e)^3 m_e}}\exp\left(\frac{E}{kT_e}\right)\sigma_e(E)\,\mathrm{d}E \tag{1}$$

$$k_{ion}^q \approx \sigma_{ion}(eV)\sqrt{\frac{2qV_D}{M}} \tag{2}$$

where E in Eqn. (1) is the energy of the electron undergoing collision and V_D in Eqn. (2) is the discharge voltage and M is the mass of a xenon atom. Equation 1 is numerically integrated using tabulated values for $\sigma_e(E)$. Assuming quasi-neutrality, the intensity of a particular transition is then

$$I(\lambda) = \frac{hc}{4\pi\lambda}n_0 n_e\left(k_e + (1-\alpha)k_{ion}^1 + \frac{\alpha}{\sqrt{2}}k_{ion}^2\right) \tag{3}$$

where α is the ratio of singly charged ion densities. While it is imperative to include the heavy particle collision excitation terms in the high-density, low T_e region of interest, there is negligible sensitivity to α since the excitation of the Xe I levels is similar regardless of the heavy particle collision. In some respects this is unfortunate since it precludes estimating α via T_e parameterization. The ratio of two lines is

$$\frac{I_1}{I_2} = \frac{\left(k_e + (1-\alpha)k_{ion}^1 + \frac{\alpha}{\sqrt{2}}k_{ion}^2\right)_1}{\left(k_e + (1-\alpha)k_{ion}^1 + \frac{\alpha}{\sqrt{2}}k_{ion}^2\right)_2}\frac{\lambda_2}{\lambda_1} \tag{4}$$

which can be used to calculate the electron temperature given I_1 and I_2.

III. Results and Discussion

Prior to testing, the cathode was conditioned by applying current to the heaters to remove impurities. Cathode ignition was performed by powering the heater elements for a prescribed period of time, applying xenon flow, then applying a high voltage across the keeper and cathode. Once ignited, the heaters were turned off and a constant keeper current of 1 A was maintained at all operating conditions.

Results are presented for cathode operation in both the "spot" and "plume" mode. Visually, spot mode operation is typically characterized by a bright, high-density plasma at the keeper/cathode orifice while plume mode consists of a widely divergent plasma. For the purposes of this work, spot mode was defined as quiescent operation with low-amplitude oscillations in the discharge current and voltage (as illustrated in Section III), Plume mode is characterized by a marked increase in the discharge voltage and accompanied by high-frequency oscillations with an amplitude orders of magnitude times higher than spot mode operation. Plume mode operation has been shown to yield high-energy ions and higher insert temperatures, both of which are life-reducing. Hysteresis effects influenced the mode of the HCA. As such, data at the flow rate of 46 sccm and a discharge current of 50 A are presented in both plume and spot mode.

Several investigations have characterized the plasma oscillations associated with hollow cathodes operating in diode (keeper only) mode, triode (keeper and anode) mode, and with Hall effect thrusters. In the context of the latter, cathode oscillations are sometimes relegated to be high-frequency ($\sim$ MHz), low amplitude oscillations which are imposed on the lower-frequency (10s to 100s of kHz) large amplitude oscillations of the discharge plasma. Both ion thruster discharge cathodes and cathodes used with Hall thrusters operate under conditions that may not be described as either spot or plume mode. The plasma is characterized by

a well-formed, extended region of high-density plasma and modest oscillations (several percent of applied voltages or currents) at 10s of kH. Therefore, additional anode configurations should be tested to establish the sensitivity of the plasma structure to the current approximation (i.e. cylindrical molybdenum anode) of a Hall thruster plasma/electron coupling environment. Further work is necessary to see if the cathode to beam coupling can be approximated in a more reasonable fashion than was implemented in this investigation.

A. Baseline Operation

The HCA was operated at discharge currents of 50, 70, and 100 A and flow rates of 19, 28, 37, and 46 sccm. These operating conditions were chosen to be consistent with nominal Hall thruster operating conditions and prior HCA testing.[10] Operation with the applied magnetic field is presented in the next section. The discharge voltage and cathode-to-ground voltage are plotted as a function of mass flow rate in Fig. 4. The decrease in discharge voltage as the flow rate is increased is characteristic of hollow cathode operation and was expected.[21–23] The cathode-to-ground potential, which is related to the ease in which electrons flow from cathode to anode, decreases with increasing flow rate. This trend is consistent with prior cathode experiments.[10,24,25]

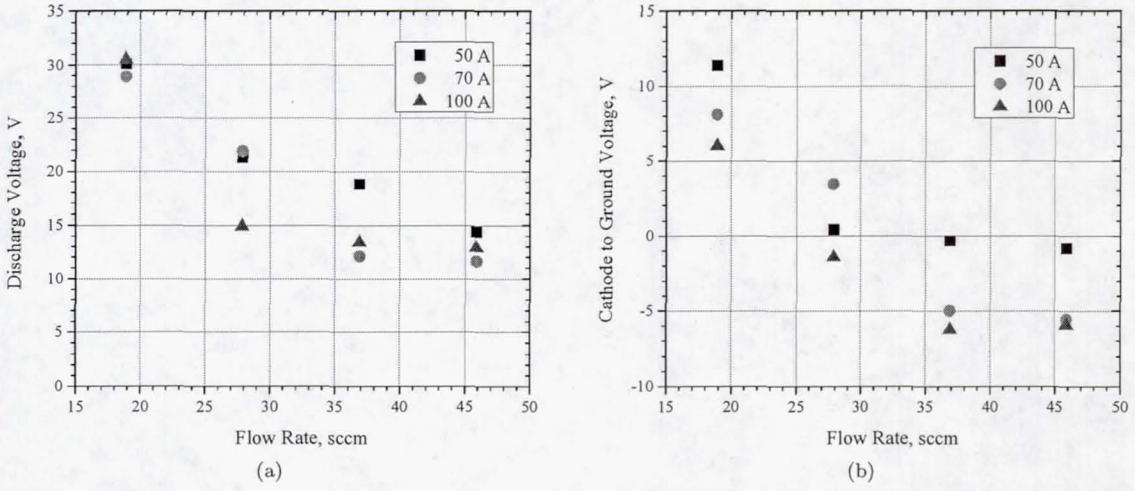

Figure 4: (a) Discharge voltage and (b) cathode to ground voltage as a function of xenon flow rate.

A photograph of the HCA operating in plume mode is shown in Fig. 5. As the flow rate is increased the plasma transitions into a collimated jet and eventually transitions to spot mode, which is characterized by a sharp decrease in discharge voltage and reduced plasma oscillations. Radial Langmuir probe sweeps for the $I_D = 50$ A case in both spot mode (46 sccm) and plume mode (19 sccm) are shown in Fig. 6. The probe is located 4 cm axially from the face of the keeper, and the $r = 0$ position is defined as the centerline. The same data for $I_D = 100$ A are shown in Fig. 7 and are largely the same. In both cases, plume mode operation yielded constant electron temperatures that were roughly 2-3$\times$ higher than spot mode operation. The plasma potential (measured with respect to ground) at the edge of the anode ($r = 10$ cm) was roughly at the discharge potential and slowly decreased as the probe was moved towards the centerline. Prior experimenters[4] have found a steep decrease in plasma potential within a centimeter of the centerline. Unfortunately, data within this region (in plume mode) could not be resolved as the data was too noisy for accurate analysis. The larger error bars in the plume mode data are associated with the high frequency oscillations present in the obtained probe data.

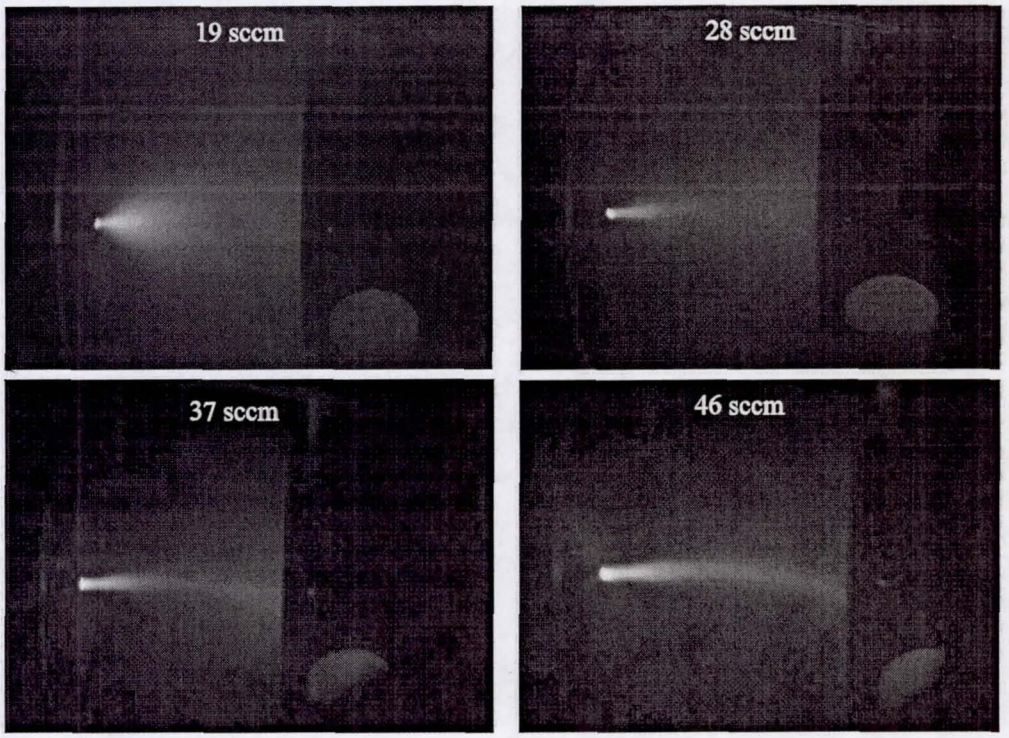

Figure 5: Plume mode operation at various flow rates at a discharge current of 50 A.

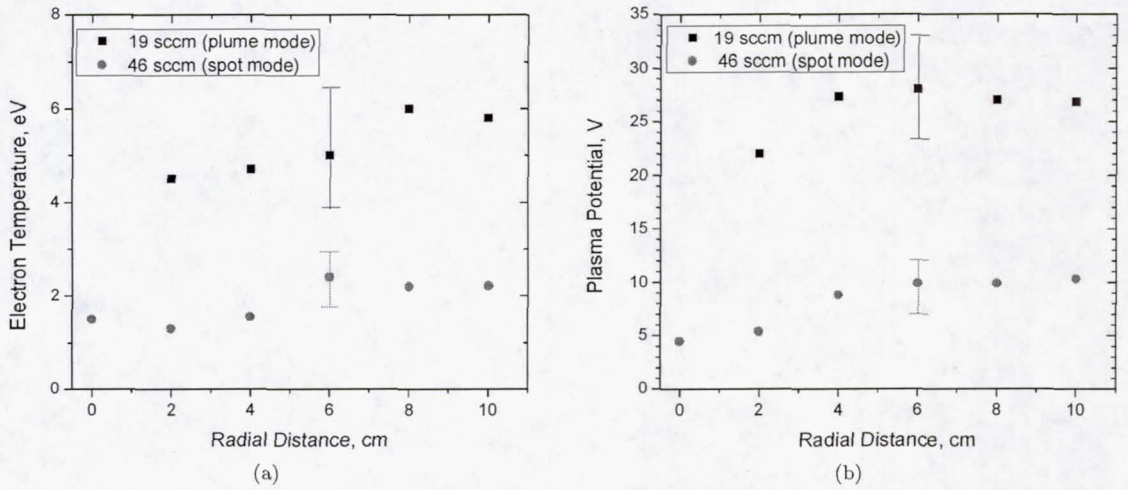

Figure 6: Langmuir probe scans of the (a) electron temperature and (b) plasma potential at a discharge current of 50 A.

Figure 8 shows the frequency characteristics of the HCA operating at 50 A, and 46 sccm. The discharge current, voltage, and keeper voltage all have oscillations at 50 kHz with peak-to-peak values of 1 A, 1 V, and 0.2 V respectively. Similar characteristics are present for spot mode operation at 70 A and 100 A.

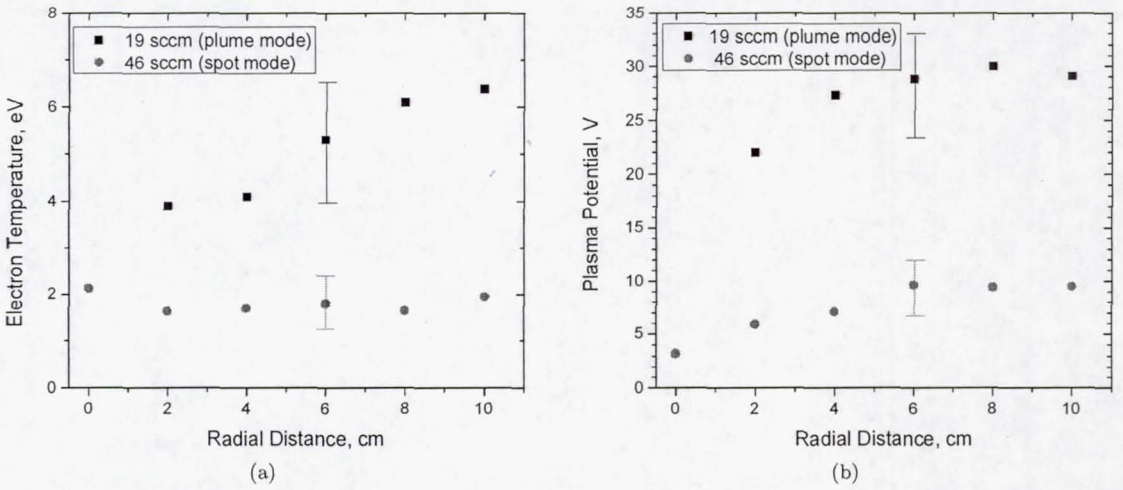

Figure 7: Langmuir probe scans of the (a) electron temperature and (b) plasma potential at a discharge current of 100 A.

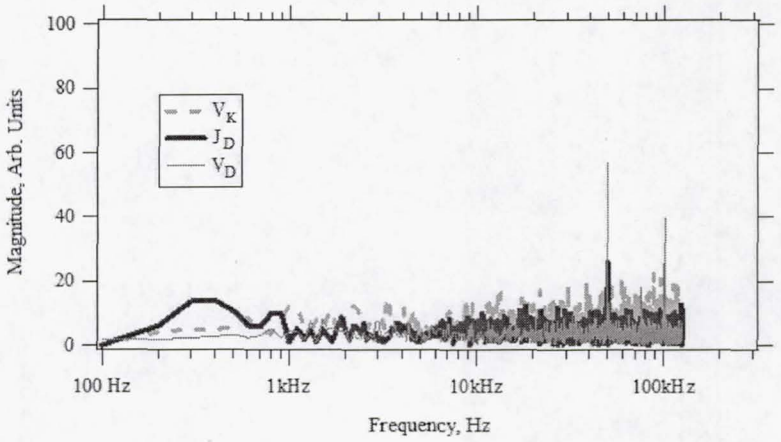

Figure 8: Frequency characterization of the HCA at 50 A, 46 sccm (during spot mode operation). Note the low amplitude and high-frequencies of the oscillations.

Plume mode operation is typically characterized by relatively high-amplitude oscillations on the order of the discharge current and voltage. Figure 9 shows the frequency characteristics of the HCA operating at 50 A and 19 sccm without an applied magnetic field. The discharge current, voltage, and keeper voltage all have oscillations at 20 to 40 kHz with peak-to-peak values of 10 A, 25 V, and 8 V, respectively. These oscillations are consistent with plume mode operation. The discharge current also has a strong oscillation at 1 kHz with a peak-to-peak value of 20 A. This low-frequency oscillation is likely a power supply related mode. This ambiguity can be eliminated with a low-frequency filter such as those used to protect the power supply during ground testing of high-power HETs. The keeper voltage has an oscillation around 150 kHz not present in the anode voltage or discharge current with a peak-to-peak value of 2 V. This additional mode is seen only in V_K oscillations (not in I_D nor V_D) in plume mode without an applied magnetic field.

The electron temperature was calculated from 823 nm and 828 nm emission at the orifice of the keeper using Eqn. 4. The calculated temperature is insensitive to the initial guess of α ($0 < \alpha < 1$). The near infrared lines are relatively free from contributions of Xe II emission. Figure 10 shows T_e as a function of mass flow rate for three discharge currents. While the uncertainty in the emission strengths is $< 1\%$, there is at least 20% uncertainty in the fit of Eqn. 4 to T_e. In addition, Karabadzhak[16] has shown a factor of 2 impact of metastable populations. However, these have greater impact for 5 eV $< T_e <$ 20 eV. For the low

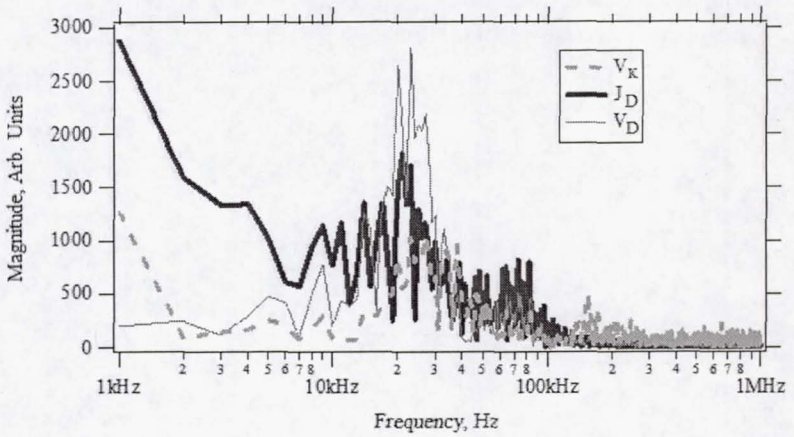

Figure 9: Frequency characterization of the HCA at 50 A and 19 sccm (plume mode). Note the presence of oscillations between 20 and 40 kHz.

T_e of this investigation, the impact of the heavy particle excitation (k^q_{ion}) is more significant than that of the metastable populations. In this light, the trend is within the uncertainty of the measurement, and the electron temperature appears roughly constant over the range of operating conditions at 2.3 eV. This result is consistent with Langmuir probe measurements of T_e in the near field of lower-power cathodes which have shown that T_e for plume mode operation increases with distance away from the orifice but is roughly the same as spot mode at the orifice.[26,27]

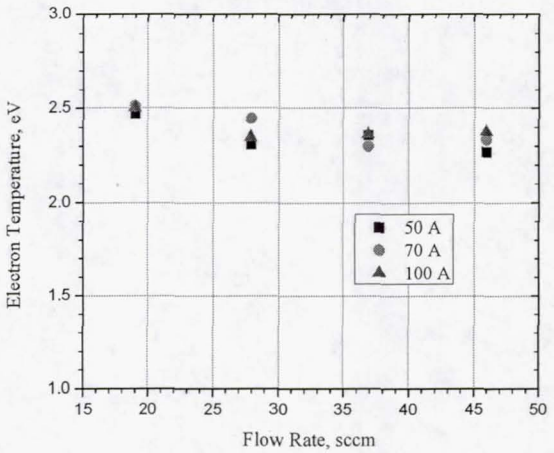

Figure 10: Electron temperature from OES at the keeper orifice as a function of mass flow rate.

Since the electron temperature is roughly constant under all operating conditions at the point of optical interrogation, the changes in emission intensity of the singly and doubly charged ions yields a qualitative measure of relative densities. Because collisional excitation coefficients (k^q_{ion}) of these lines are unknown, it is still inappropriate to use the ratios to accurately estimate the charge state ratio, α. However, the ratio of emission intensities of doubly to singly charged ions should still yield a good qualitative measure of the degree of doubly charged ion production at the keeper orifice assuming $T_e \approx$ constant. Figure 11 shows the ratio $I_{\text{Xe III, 278 nm}}$ to $I_{\text{Xe II, 286 nm}}$ as a function of mass flow rate for three discharge currents. There are significantly higher fractions of Xe III at the lower flow rates, especially for $I_D = 50$ A and 70 A. These conditions are clearly in plume mode based on the observed oscillations described above. The variation in values at 46 sccm give a sense of the point-to-point uncertainty in these ratios. Larger uncertainty exists at

the lowest flow rate.

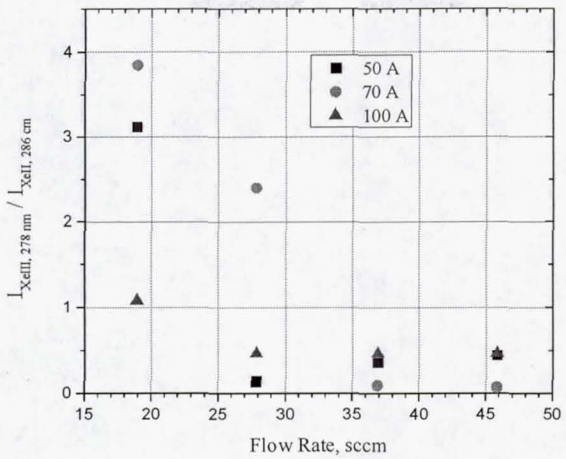

Figure 11: $I_{\text{Xe III, 278 nm}}$ to $I_{\text{Xe II, 286 nm}}$ as a function of mass flow rate. The ratio provides an indication of the relative concentrations of Xe III and Xe II since $T_e \approx$ constant.

Figure 12 shows the variation in the self-normalized $I_{\text{C II, 299 nm}}$ signal measured at the keeper orifice as a function of flow rate for the three discharge currents. Note that there is negligible signal for both the 50 A and 70 A conditions above 30 sccm and that the value is non-zero for all 100 A conditions. However, as expected, the signal is the highest at lowest flow rates, which are associated with plume mode. Without a reasonably good model for the excitation of the C II state, it is not possible to quantitatively correlate the signal strength with the amount of carbon being eroded from the surface. However, as with Xe II and Xe III, a constant T_e removes a large source of the uncertainty and allows for some correlation. The C I emission was not observed at any of the operating conditions without a magnetic field. Perhaps this is because the carbon atoms are being quickly ionized as V_D is well above the ionization potential of 12 eV.

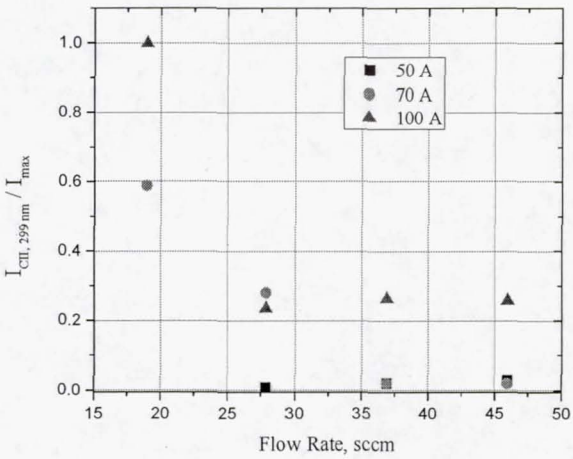

Figure 12: Self-normalized $I_{\text{C II, 299 nm}}$ signal measured at the keeper orifice as a function of flow rate.

Ion energy distributions measured with the axial RPA are shown in Fig. 13 for a discharge currents of 50 and 100 A at a flow rate of 46 sccm with the HCA operating in spot mode. The RPA bias voltage is corrected by subtracting off the local plasma potential; this is done because the RPA bias voltage was swept with respect to facility ground. The peak energies are within a few volts of the discharge voltage, and the energy distribution is relatively narrow. The radially positioned RPA yielded unphysical results during spot mode operation; this is likely due to a lack of directed ions reaching the probe. Decreasing the flow rate to 19 sccm yielded the transition to plume mode, which was accompanied by much wider ion distributions, as

shown in Figs. 14 - 16. Similar results have been reported by Goebel et al.,[5] who postulated that a plasma structure is established which couples with the oscillations to yield the high energy ion distributions. The variation in the ion energy in the radial direction from 70 A to 100 A may occur because the ionization region is moving, perhaps simply extending, downstream.

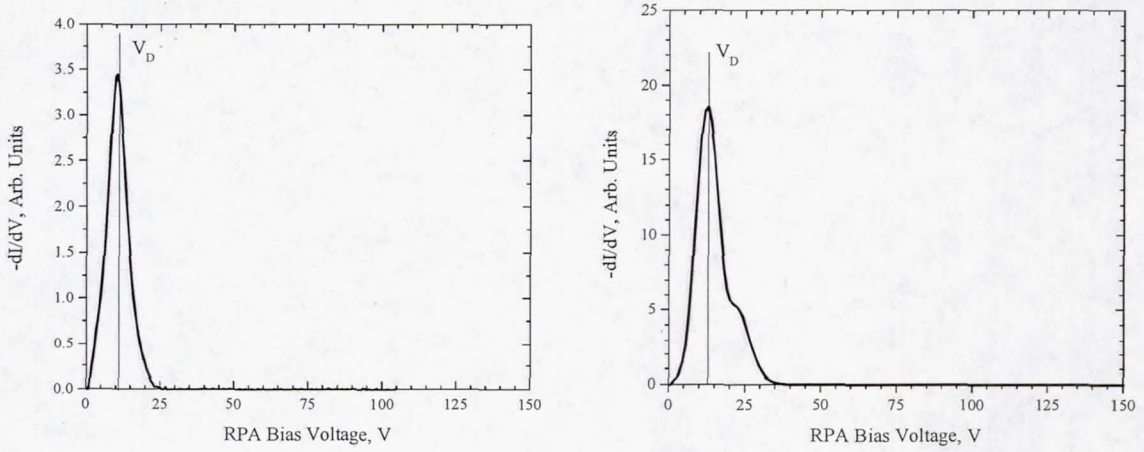

Figure 13: Ion energy distribtion for the cathode operating at (a) 50 A and (b) 100 A at a flow rate of 46 sccm utilizing the axially positioned RPA. The vertical lines denote the discharge voltage.

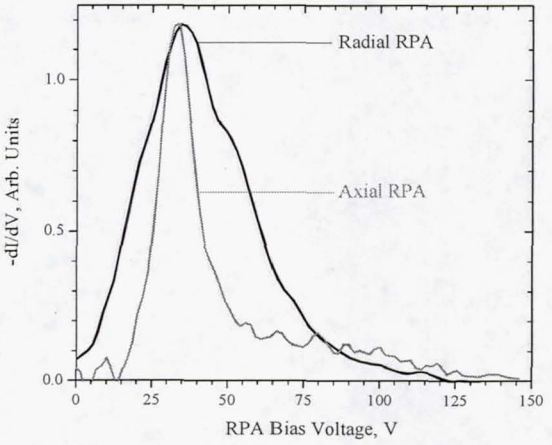

Figure 14: Ion energy distribution for 50 A and 19 sccm (plume mode).

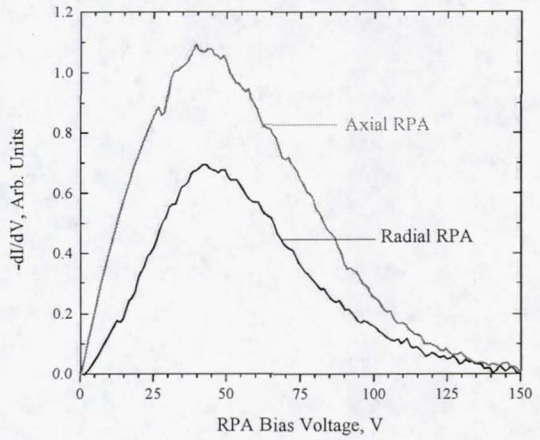

Figure 15: Ion energy distribution for 70 A and 19 sccm (plume mode).

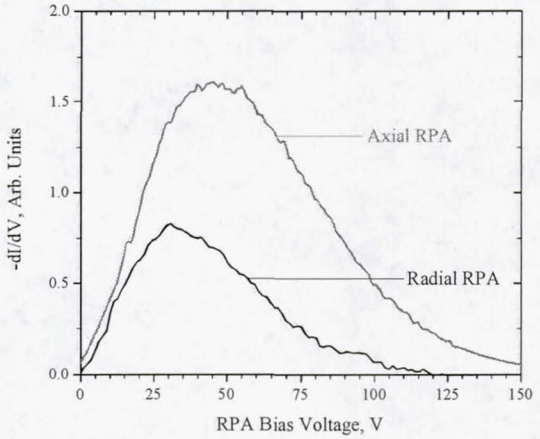

Figure 16: Ion energy distribution for 100 A and 19 sccm (plume mode).

B. Applied Magnetic Field Operation

Data was obtained at 5 different magnetic field strengths. The data are normalized by a magnetic field strength B_o characteristic of thruster operation at full power. There was a pronounced difference in HCA operation when the magnetic field was applied. A photograph of the HCA operating at 100 A with and without the magnetic field is shown in Fig. 17. The plume emanating from the HCA forms a jet-like structure as the electrons follow the applied field, which is primarily axial along the centerline.

The discharge voltage and cathode-to-ground voltage are plotted as a function of magnetic field strength for a mass flow rate of 46 sccm (spot mode) in Fig. 18. The discharge voltage increases monotonically with the magnetic field strength. This is likely due to the increased power necessary to complete the circuit, as the current can only be collected at the anode if the electrons diffuse across the primarily axial B-field. Unfortunately, the Langmuir probe data with an applied magnetic field configuration could not be accurately analyzed due to excessive oscillations in the collected probe signals. Additionally, limited data was obtained at lower flow rates as the discharge voltage exceeded the output capability of the discharge power supply.

Figure 19 shows the variation in T_e, as measured by OES at the keeper orifice as a function of normalized applied magnetic field strength. There is no difference in T_e with flow rate or I_D for $B_o > 0$. The electron temperature increases slightly as the field strength is increased and then becomes constant. This increase exceeds the measurement uncertainty (20%) and potentially results from the constrained flow of the electrons as evidenced by the low-frequency oscillations present with applied fields.

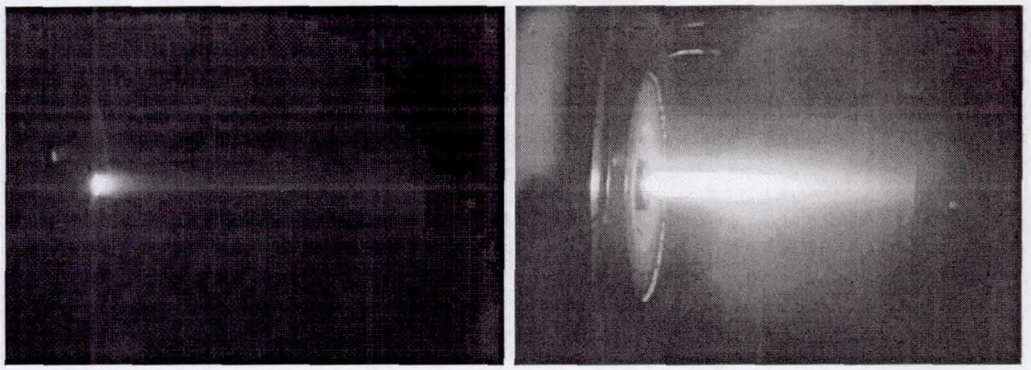

Figure 17: Cathode operating in spot mode (left) and with applied magnetic field (100 A, 46 sccm, $B = B_o$).

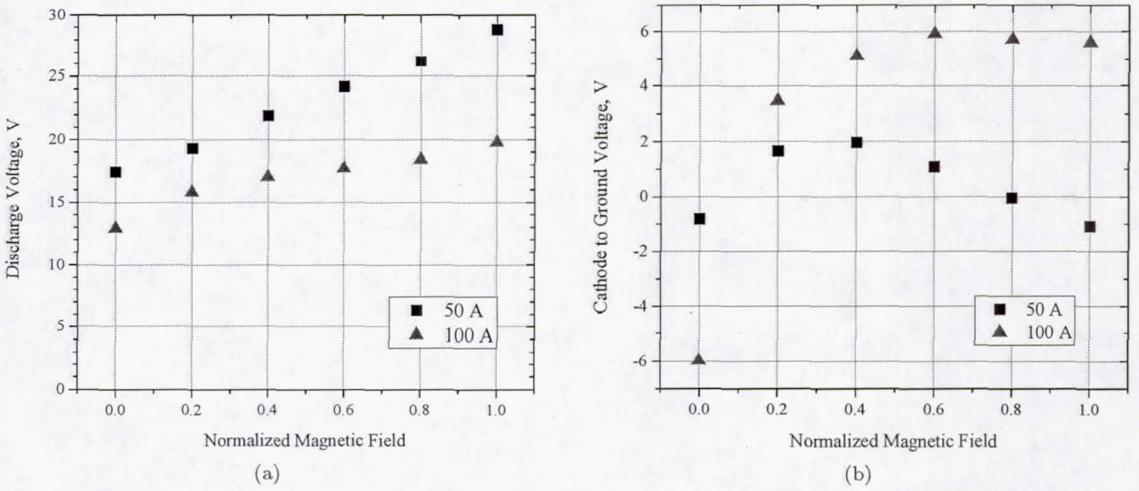

Figure 18: (a) Discharge voltage and (b) cathode to ground voltage as a function magnetic field strength for a flow rate of 46 sccm at discharge currents of 50 A and 100 A.

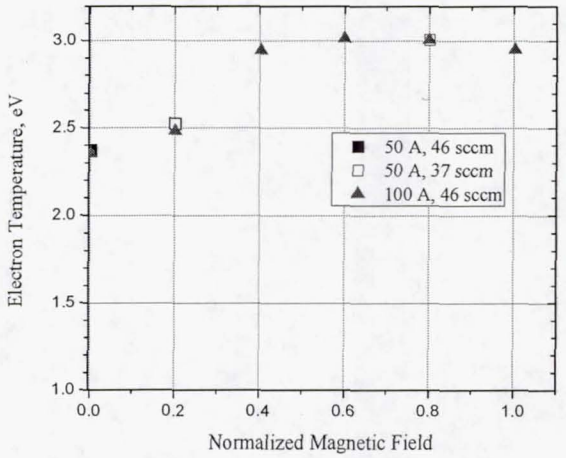

Figure 19: Electron temperature obtained from from OES at the keeper orifice as a function of normalized applied magnetic field strength for three cathode operating conditions.

Figure 20 shows the ratio of $I_{\text{Xe III, 278 nm}}$ to $I_{\text{Xe II, 286 nm}}$ as a function of normalized applied magnetic field for three operating conditions. The difference in trend between the 50 A and the 100 A cases extends slightly above the uncertainty in the measurement. Despite nearly an identical T_e, V_D and oscillatory behavior, the formation of Xe III ions appears to increase significantly for the 100 A case with respect to the 50 A cases. This trend may suggest that there are fundamentally different phenomena associated with the large scale, low-frequency oscillations during applied magnetic fields and the oscillations typical of plume mode operation. The increase in the intensity ratios for both 50 and 100 A operation likely results from a combination of increasing T_e and n_e and therefore may or may not reflect changes in Xe II and Xe III densities. However, above $B_o = 0.4$, the electron temperature is constant suggesting changes are related to densities.

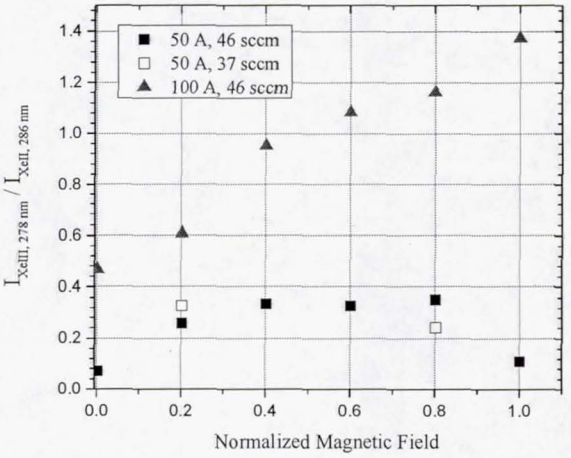

Figure 20: $I_{\text{Xe III, 278 nm}}$ to $I_{\text{Xe II, 286 nm}}$ as a function of normalized applied magnetic field for three operating conditions

Figure 21 shows the self-normalized $I_{\text{C I 833 nm}}$ and $I_{\text{C II, 299 nm}}$ signal strengths as a function of normalized applied magnetic field for the 100 A operating condition. With an applied magnetic field, the C I line at 833.5 nm becomes significant. At 50 A, the signal-to-noise ratio is low except at the highest B-fields. This suggests that Xe III may be responsible for most of the carbon erosion which is consistent with the large sputter threshold of Xe II on carbon.

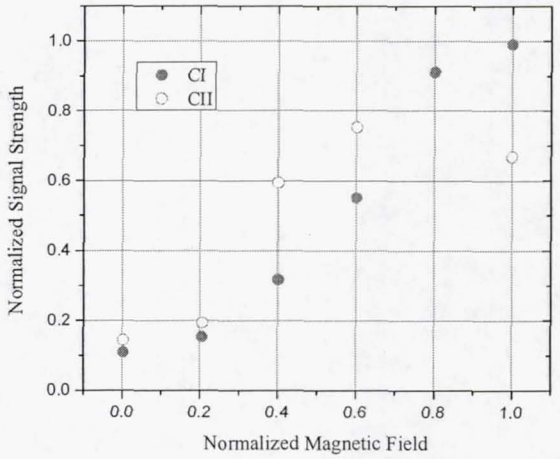

Figure 21: Self-normalized $I_{\text{C I 833 nm}}$ and $I_{\text{C II, 299 nm}}$ signal strengths as a function of normalized applied magnetic field for the 100 A operating condition.

Figure 22 shows the frequency characteristics of the HCA operating at 50 A and 37 sccm with an applied

magnetic field of $0.6B_o$. The discharge and keeper voltages all have oscillations between 20 to 40 kHz with peak-to-peak values of 20 V, and 2 V respectively. Both are consistent with plume mode operation even though the flow yielded spot mode characteristics without the applied magnetic field. Most notable, however, are the absence of I_D peaks at these frequencies and a very large 70 A peak-to-peak oscillation at 1 kHz. The keeper voltage also has an oscillation at 1 kHz with a peak-to-peak value of 1 V. The very large oscillation of I_D at 1 kHz and modest V_D and V_K oscillations around 30 kHz are present for all applied-field operating conditions regardless of mass flow rate. At lower applied fields and at higher flow rates, the magnitudes of all of the oscillations decrease, but the I_D oscillation never decreases below 0.5 I_D in peak-to-peak value.

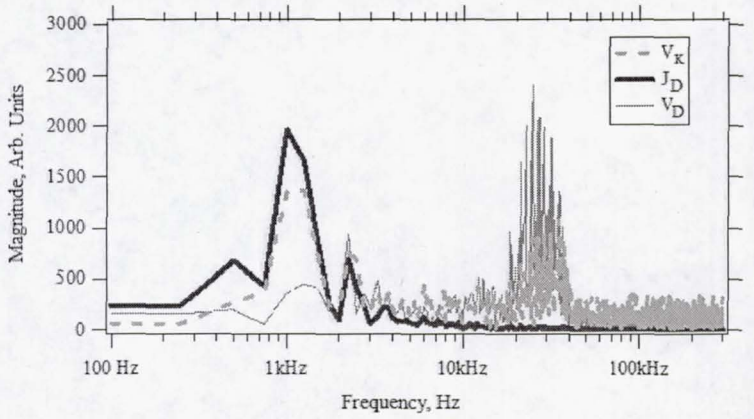

Figure 22: Frequency characterization of the HCA at 50 A, 37 sccm, and $0.6B_o$. Note the large oscillation at 1 kHz and the absence of oscillations at higher frequencies for I_D.

To measure the luminosity of the plasma, an optical probe focused just downstream of the keeper orifice focused light on a high-speed photodiode. The output of the diode had identical frequency characteristics to I_D when the magnetic field was applied: large oscillations at 1 kH, suggesting the plasma was extinguishing at the cathode.

The ion energy distribution for an applied field of $0.2B_o$ and $0.4B_o$ at a discharge current of 50 A is shown in Fig. 23. In both cases the on-axis RPA detects a narrower range of ion energies, with the radial probe detecting ions several factors higher than the discharge voltage. Identical trends have been reported with HCAs in the presence of magnetic field.[4–6] Goebel et al. postulated that turbulent acoustic fluctuations and ionization instabilities are responsible for the creation of the high-energy ions.

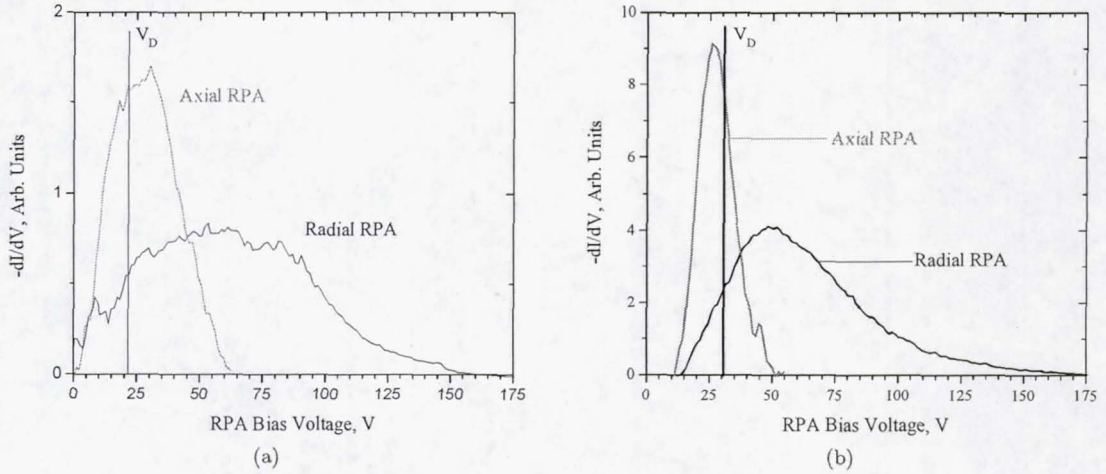

Figure 23: Ion energy distribution for a discharge current of 50 A with an applied magnetic field strength of (a) $0.2B_o$ and (b) $0.4B_o$.

IV. Conclusions

Plasma plume measurements have been reported for a hollow cathode assembly operated at discharge currents of 50-100 A at flow rates between 19 and 46 sccm. The HCA is centrally mounted in NASA-300MS Hall Thruster, which utilizes a magnetic field configuration designed to significantly limit discharge channel wall erosion. Ion energy distributions, emission spectra, and high-frequency oscillations have been reported for operation with and without an applied magnetic field. Spot mode operation was characterized by low-amplitude oscillations, an electron temperature of 2 eV near the keeper orifice plate, and relatively narrow ion energy distributions centered around the discharge voltage. Decreasing the flow rate yielded plume mode operation, which was characterized by high-frequency, large-amplitude oscillations and electron temperatures on the order of 5-6 eV away from the keeper orifice (but still on the order of 2.3 eV at the orifice). When the magnetic field was applied, the HCA transitioned from spot mode to an intense beam mode with plume-like oscillations in the discharge and keeper voltages and large, 1 kHz oscillations in the discharge current.

Retarding potential analyzers placed both on-axis and 90 degrees off axis yielded ion energies significantly in excess of the discharge voltage. Plume mode operation yielded broad distributions of ion energies in both the axial and radial directions, consistent with previous investigations. Operating in nominally spot-mode conditions with an applied field yielded relatively narrow ion energy distributions on-axis. This, too, is consistent with recent investigations. Decreases in the collector current and spread of the high-energy ions as the magnetic field was increased for a given operating condition suggests that the plasma structure generating the ions is changing. Detailed, time sensitive measurement of the ion energies and plasma conditions will be required to further resolve the structures.

Optical emission spectra were collected to measure electron temperature, relative xenon charge states, and the relative amount of carbon sputtered from the keeper. The electron temperature was shown to be constant in the very near-field of the keeper orifice and this allowed qualitative assessment of the charge states and sputtered carbon. Application of an applied magnetic field increased both the amount of Xe III in the orifice region and the amount of C emission. Since the two correlated well with operating condition, the bulk of the carbon sputtering was likely due to Xe III. Both increased linearly with applied magnetic field for 100 A operation but were constant at 50 A and 70 A operation at the same flow rates. This suggests a significant increase in keeper erosion for higher current operation if the cathode flow rate is not proportionately higher.

Acknowledgments

The authors would like to thank and acknowledge the Office of the Chief Technologist for funding this work as well as Timothy Smith for serving as the Project Manager. The authors thank Mike Pastel and Kevin McCormick for their aid in manufacturing and testing of the high current cathode assemblies. The authors also thank Rohit Shastry and Wensheng Huang for their contributions in setting up the plasma diagnostics.

References

[1]Kamhawi, H., Haag, T., Jacobson, D., and Manzella, D., "Performance Evaluation of the NASA 300M 20 kW Hall Effect Thruster," 47^{th} *AIAA/ASME/SAE/ASEE Joint Propulsion Conference & Exhibit*, AIAA-2011-5521, July 2011.

[2]Soulas, G., Haag, T., Herman, D., Huang, W, K. H., and Shastry, R., "Performance Test Results of the NASA-457Mv2 Hall Thruster," 48^{th} *AIAA/ASME/SAE/ASEE Joint Propulsion Conference & Exhibit*, AIAA-2012-3940, July 2012.

[3]Kamhawi, H., "Performance and Thermal Characterization of the 20 kW 300MS Hall Effect Thruster," 33^{rd} *International Electric Propulsion Conference*, IEPC-2013-444, Oct. 2013.

[4]Jameson, K., Goebel, D., and Watkins, R., "Hollow Cathode and Keeper-Region Plasma Measurements," 41^{st} *AIAA/ASME/SAE/ASEE Joint Propulsion Conference & Exhibit*, AIAA-2005-3667, July 2012.

[5]Goebel, D., Jameson, K., Katz, I., and Mikellides, I., "Energetic Ion Production and Keeper Erosion in Hollow Cathode Discharges," 29^{th} *International Electric Propulsion Conference*, IEPC-2005-266, Oct. 2013.

[6]Goebel, D. and Chu, E., "High Current Lanthanum Hexaboride Hollow Cathode for 20-to-100 kW Class Hall Thrusters," 48^{th} *AIAA/ASME/SAE/ASEE Joint Propulsion Conference & Exhibit*, AIAA-2012-4079, July 2012.

[7]Williams, G. J., Smith, T. B., Domonkos, M. T., Shand, K. J., Gallimore, A. D., and Drake, R. P., "Laser Induced Fluorescence Characterization of Ion Emitted from Hollow Cathode," 35^{th} *AIAA/ASME/SAE/ASEE Joint Propulsion Conference & Exhibit*, AIAA-1999-2862, June 1999.

[8]Williams, G., Smith, T., Glick, K., Hidaka, Y., and Gallimore, A., "FMT-2 Discharge Cathode Erosion Rate Measurements Via Laser-Induced Fluorescence," 36^{th} *AIAA/ASME/SAE/ASEE Joint Propulsion Conference & Exhibit*, AIAA-2000-3663, July 2000.

[9]Sengupta, A., Brophy, J., and Goodfellow, K., "Status of the Extended Life Test of the Deep Space 1 Flight Spare Ion Engine After 30,352 Hours of Operation," 39^{th} *AIAA/ASME/SAE/ASEE Joint Propulsion Conference & Exhibit*, AIAA-2003-4558, July 2003.

[10]Kamhawi, H. and Van Noord, J., "Development and Testing of High Current Hollow Cathodes for High Power Hall Thrusters," 48^{th} *AIAA/ASME/SAE/ASEE Joint Propulsion Conference & Exhibit*, AIAA-2012-4080, July 2012.

[11]Mikellides, I., Katz, I., Hofer, R., Goebel, D., de Grys, K., and Mathers, A., "Magnetic Shielding of the Channel Walls in a Hall Plasma Accelerator," *Physics of Plasmas*, Vol. 18, No. 3, 2011, 033501.

[12]Huang, W., Shastry, R., Soulas, G., and Kamhawi, H., "Farfield Plume Measurement and Analysis on the NASA-300M and NASA-300MS," 33^{rd} *International Electric Propulsion Conference*, IEPC-2013-057, Oct. 2013.

[13]Shastry, R., Huang, W., Soulas, G., and Kamhawi, H., "Langmuir Probe Measurements within the Discharge Channel of the 20 kW NASA-300M and NASA-300MS Hall Thrusters," 33^{rd} *International Electric Propulsion Conference*, IEPC-2013-122, Oct. 2013.

[14]Kozintseva, M., "Forecast of Erosion Rate of SPT K-0 Channel Insulators by Spectral Measurements," 32^{nd} *International Electric Propulsion Conference*, IEPC-2011-293, Sept. 2011.

[15]Hargus, W., "Optical Boron Nitride Insulator erosion Characterization of a 200 W Xenon Hall Thruster," 41^{st} *AIAA/ASME/SAE/ASEE Joint Propulsion Conference & Exhibit*, AIAA-2005-3529, July 2012.

[16]Karabadzhak, G. and Semenkin, A., "Evaluation of a Xenon Operating Hall Thruster Body Erosion Rate Through Analysis of Its Optical Spectra," 37^{th} *AIAA/ASME/SAE/ASEE Joint Propulsion Conference & Exhibit*, AIAA-2001-3889, July 2001.

[17]Williams, G., Soulas, G., and Kamhawi, H., "Advanced Diagnostic Characterization of High-Power Hall Thruster Wear and Operation," 48^{th} *AIAA/ASME/SAE/ASEE Joint Propulsion Conference & Exhibit*, AIAA-2012-4036, July 2012.

[18]Shastry, R., Huang, W., Herman, D., Soulas, G., and Kamhawi, H., "Plasma Potential and Langmuir Probe Measurements in the Near-field Plume of the NASA-457Mv2 Hall Thruster," 48^{th} *AIAA/ASME/SAE/ASEE Joint Propulsion Conference & Exhibit*, AIAA-2012-4196, July 2012.

[19]Hutchinson, I., *Principles of Plasma Diagnostics, 2nd Addition*, Cambridge University Press, 2002.

[20]Chiu, Y. H., "Passive Optical Diagnostic of Xe Propelled Hall Thrusters, Part 1: Emission Cross Sections," *Journal of Applied Physics*, Vol. 99, No. 11, 2006, 113304.

[21]John, J., Sarver-Verhey, T., and Kamhawi, H., "High Current Cathode Development for 50 kW Class Hall Thruster," 41^{st} *AIAA/ASME/SAE/ASEE Joint Propulsion Conference & Exhibit*, AIAA-2005-4244, July 2005.

[22]Noord, J. V., Kamhawi, H., and McCwen, H., "Characterization of a High Current, Long Life Hollow Cathode," 27^{th} *International Electric Propulsion Conference*, IEPC-2001-321, Oct. 2001.

[23]Carpenter, C. and Patterson, M., "High-Current Hollow Cathode Development," 27^{th} *International Electric Propulsion Conference*, IEPC-2001-274, Oct. 2001.

[24]Goebel, D., Jameson, K., Katz, I., and Hofer, R., "Hall Thruster Cathode Flow Impact on Coupling Voltage and Cathode Life," *Journal of Propulsion and Power*, Vol. 28, No. 2, 2012, pp. 355–363.

[25]Tilley, D., deGrys, K., and Myers, R., "Hall Thruster Cathode Coupling," 35^{th} *AIAA/ASME/SAE/ASEE Joint Propulsion Conference & Exhibit*, AIAA-1999-2865, June 1999.

[26]Williams, G., Domonkos, M., Shand, K., Haas, J., King, L., and Gallimore, A., "Near-field Investigation of Ions Emitted from a Hollow Cathode Assembly Operating at Low Power," 34^{th} *AIAA/ASME/SAE/ASEE Joint Propulsion Conference & Exhibit*, AIAA-1998-3658, July 1998.

[27]Martin, R. and Williams, J., "Direct Measurements of Plasma Properties nearby a Hollow Cathode Using a High Speed Electrostatic Probe," 42^{nd} *AIAA/ASME/SAE/ASEE Joint Propulsion Conference & Exhibit*, AIAA-2006-4820, July 2006.